NASA CONTRACTOR
REPORT

NASA CR-129004

ATMOSPHERIC EFFECTS ON REMOTE SENSING OF NON-UNIFORM TEMPERATURE SOURCES

By W. A. McNeill, J. M. Elliott, and B. P. Dixon

Department of Mechanical Engineering
Division of Engineering
University of South Alabama
Mobile, Alabama 36688

May 22, 1973

Prepared for

NASA-GEORGE C. MARSHALL SPACE FLIGHT CENTER
Marshall Space Flight Center, Alabama 35812

TECHNICAL REPORT STANDARD TITLE PAGE

1. REPORT NO.	2. GOVERNMENT ACCESSION NO.	3. RECIPIENT'S CATALOG NO.
NASA CR-129004		

4. TITLE AND SUBTITLE
ATMOSPHERIC EFFECTS ON REMOTE SENSING OF NON-UNIFORM TEMPERATURE SOURCES

5. REPORT DATE
May 22, 1973

6. PERFORMING ORGANIZATION CODE

7. AUTHOR(S)
W. A. McNeill, J. M. Elliott, and B. P. Dixon

8. PERFORMING ORGANIZATION REPORT #

9. PERFORMING ORGANIZATION NAME AND ADDRESS
Department of Mechanical Engineering
Division of Engineering
University of South Alabama
Mobile, Alabama 36688

10. WORK UNIT NO.

11. CONTRACT OR GRANT NO.
Contract NAS8-28722

12. SPONSORING AGENCY NAME AND ADDRESS
Aerospace Environment Division
Aero-Astrodynamics Laboratory
George C. Marshall Space Flight Center
Marshall Space Flight Center, Alabama 35812

13. TYPE OF REPORT & PERIOD COVERED
Contractor
April 13, 1972 - Feb. 28, 1973.

14. SPONSORING AGENCY CODE

15. SUPPLEMENTARY NOTES
This work performed under the direction of the Aerospace Environment Division, Aero-Astrodynamics Laboratory, Science and Engineering Directorate.

16. ABSTRACT

The equations of transfer, for a plane-parallel scattering atmosphere with a point source of energy on the lower bounding surface, have been solved for various values of sensor/point source orientation and optical depths. Applications of this analysis to SKYLAB and ERTS missions are discussed, and requirements for atmospheric property data and radiation transfer properties are considered.

17. KEY WORDS
Remote Sensing
Atmospheric Effects
Radiant Energy
Scattering
Absorption

18. DISTRIBUTION STATEMENT
PUBLIC RELEASE:

E. D. Geissler
Director, Aero-Astrodynamics Laboratory

19. SECURITY CLASSIF. (of this report)	20. SECURITY CLASSIF. (of this page)	21. NO. OF PAGES	22. PRICE
UNCLASSIFIED	UNCLASSIFIED	36	NTIS

MSFC - Form 3292 (May 1969)

PREFACE

Various remote sensors which are designed to sense electromagnetic energy emitted by objects on the earth's surface can yield accurate results, providing the effects of the atmosphere on the energy emitted from the ground are known. Influence of the atmosphere by scattering, absorption, and emission will have some effect on the remote sensors planned for earth resources applications, such as Skylab and ERTS. It is important, therefore, that an estimate be made of this atmospheric participation with the electromagnetic energy transferred from the ground.

Accordingly, the objective of the work reported herein was to solve the equations of transfer, for a plane-parallel scattering atmosphere with a point source of energy on the lower bounding surface, for various values of sensor/point source orientation and optical depths. It is planned to consider absorption and emission effects in the transfer model in the next phases of this investigation, with the ultimate aim being to apply the study results to Skylab and ERTS experiments.

TABLE OF CONTENTS

PREFACE iii

LIST OF FIGURES v

NOMENCLATURE vi

I. INTRODUCTION 1

II. ANALYTICAL DEVELOPMENT 3
Governing Equations 4
Pure Scattering 10
Numerical Results 14
Conclusions 15

III. DISCUSSION OF RESULTS 21

IV. ATMOSPHERIC AND RADIATION TRANSFER PROPERTIES 24

V. SKYLAB EARTH SENSING EXPERIMENTS 26

VI. SUMMARY 29

REFERENCES 30

LIST OF FIGURES

1 Radiation Transfer Field Geometry 5

2 Sensor/Point Source Geometry 9

3 Dimensionless Intensity vs. R/h as Function of Optical Depth, $\theta=0°$ 16

4 Dimensionless Intensity vs. R/h as Function of Optical Depth & ϕ, $\theta=22.5°$ 17

5 Dimensionless Intensity vs. R/h as Function of Optical Depth & ϕ, $\theta=45°$ 18

6 Dimensionless Intensity vs. R/h as Function of Optical Depth & ϕ, $\theta=67.5°$ 19

7 Example Application 23

8 SKYLAB Sensor Orientation 28

NOMENCLATURE

A - Area

c - Speed of light

$e_{b\nu}$ - Black-body emissive power

E_ν - Rate of flux of radiant energy

G_ν - Incident radiation function

G^*_ν - Point-source radiation function (Equation [11])

$\bar{h}$ - Planck constant

h - Sensor altitude

I_ν - Intensity

j_ν - Emission coefficient

k - Boltzmann constant

Δm - Mass element of participating atmosphere

P - Scattering function

R - Distance from point source to sensor line-of-sight ground intercept

s - Distance coordinate locating Δm (Figures 1, 2)

T - Absolute temperature

z - Vertical coordinate (Figure 1)

$\beta_\nu, \gamma_\nu, \kappa_\nu$ - $\rho\beta'_\nu, \rho\gamma'_\nu, \rho\kappa'_\nu$, respectively

β'_ν - Extinction coefficient ($=\gamma'_\nu + \kappa'_\nu$)

γ'_ν - Scattering coefficient

Δ - Minimum value of μ (Equation [10])

$\theta, \phi; \theta', \phi'$ - Cylindrical coordinates (Figure 2)

κ'_ν - Absorption coefficient

μ - cos θ

ν - Frequency of radiant energy

ξ - Minimum value of θ (Equation [6])

ρ - Mass density of participating atmosphere

τ_ν - Optical thickness

ω - Solid angle

$\bar{\omega}$ - Scattering albedo

I. INTRODUCTION

With the increase in accuracy with which remote sensors can measure the amount of radiant energy incident on their measuring devices, it has become necessary to accurately account for the influence of the intervening atmosphere on the upwelling energy. Because radiant energy leaving the earth's surface (reflected and/or emitted energy) is attenuated due to absorption and scattering by the atmosphere, the sensor which operates at altitude does not sense the energy actually leaving the ground. The ability to correctly account for this atmospheric "participation" in the radiative transfer process is especially important when it is desired to accurately measure temperature of ground features. Temperature measurement depends on the ability to measure the amount of energy emanating from a particular feature. This energy is proportional to the 4th power of the absolute temperature of the object so that by knowing the amount of energy (and incidently knowing the proportionality constant) one could then determine the temperature. However, since the remote sensor at altitude senses a different energy level due to atmospheric attenuation of the energy, an incorrect temperature will be calculated from energy measurements.

Atmospheric models have been developed which account for this atmospheric participation in the radiative transfer but most consider the lower bounding radiating surface (corresponding to the earth's surface) to be at a constant temperature. Even with this assumption, a general analysis is extremely complex and the atmospheric models and associated property evaluation programs are very large and require extensive computer time.

The first objective of this study is to perform an analytical investigation of the effects of the atmosphere on the transfer and sensing of electromagnetic energy, considering a non-uniform earth surface temperature. Section II of this report presents in detail the analytical radiation transfer model developed to meet this objective.

The second objective is to develop the analysis so that any wavelength region may be considered. As will be shown in Section II, the general radiation transfer model is valid for all wavelengths but initial computations will be restricted to the wavelength band which closely approximates both ERTS-B and SKYLAB infrared scanners (see Section V).

Consideration of pertinent parameters influencing atmospheric participation is the third primary objective of this study. The 4-D atmospheric models [1] will be discussed relative to this study in Section IV. In addition, available radiation transport property models will be discussed in Section IV.

The fourth and final primary objective is to review the SKYLAB (and ERTS-B) earth sensing experiments relative to this study. Initial solutions of the transport equations and interpretation of results will be made for the wavelength band in which the SKYLAB and ERTS-B infrared scanners operate. The results of the present study can then be used to predict the effects of atmospheric effects on the thermal mapping of the non-uniform earth surface by SKYLAB and ERTS-B. Section V contains the information on SKYLAB and ERTS-B relative to this study.

II. ANALYTICAL DEVELOPMENT

Formulation of the radiation transfer model is initiated by considering the scattering effect of a parallel-plane atmosphere upon the radiant energy emitted, at a known intensity, by a single point source located on the surface of the earth. Results of such an analysis provide theoretical prediction of the contribution of the point source to the rate of energy received by a sensor, at some altitude, whose line-of-sight does not intercept the surface at the location of the point source. If, for example, it is desired to determine the surface temperature at the ground level line-of-sight intercept by remote sensing, energy emitted by another surface point and scattered by the aerosol into the direction of the sensor line-of-sight must be regarded as "noise", producing an error in the temperature predicted by the sensor. The results of this investigation may be employed to estimate and thereby correct sensing errors of this type.

The linearity of the governing equations employed in this investigation permits a superposition of the effects of any number of point sources, and thus provides the basis for an analysis of the effects of a scattering atmosphere upon energy emitted by a surface having a general non-uniform temperature distribution.

It is assumed that emission from the point source is diffuse, that scattering is isotropic and coherent, that thermodynamic equilibrium prevails, and that conduction and convection effects are negligible. Computations are based on an average extinction coefficient, assumed constant with altitude.

Governing Equations

Consider an elemental area ΔA and a solid angle $\Delta\omega$ having its vertex in ΔA and inclined at an angle θ with the vertical (Fig. 1). Let $\Delta E_{\nu P_1}$ be the rate of energy in the frequency range $\Delta\nu$ confined to $\Delta\omega$, crossing a horizontal plane at the point P_1. The energy rate $\Delta E_{\nu P_1}$ may in general consist of energy emitted at ΔA, emitted by the intervening atmosphere, or scattered into $\Delta\omega$. The intensity $I_{\nu P_1}$ is defined to be

$$I_{\nu P_1} \equiv \frac{\Delta E_{\nu P1}}{\cos\theta\ \Delta A\ \Delta\omega\ \Delta\nu}$$

A similar definition of intensity holds for all other points, such as P_2. Thus if there is neither scattering nor emission by the atmosphere, $I_{0\nu}=I_{\nu P_1}=I_{\nu P_2}$. The sense of I_ν is identified by writing I_ν^+ when θ is acute, and I_ν^- when θ is obtuse. At point P_1 an atmospheric slab of height $\Delta z=\Delta s\cos\theta$ associates with $\Delta\omega$ a mass element $\Delta m=P\Delta A\cos\theta\ \Delta s$. When atmospheric participation occurs, the intensity at point P_2, at the top of the slab, may be different from that at P_1 due to atmospheric emission, absorption and scattering. To describe this participation, an emission coefficient j_ν is defined such that the energy emitted by Δm per unit time, in the frequency range Δ_ν, and confined to $\Delta\omega$ is $j_\nu\Delta m\Delta\omega\Delta\nu$. Absorption of energy incident upon a mass element Δm is described in terms of an absorption coefficient κ_ν', the path

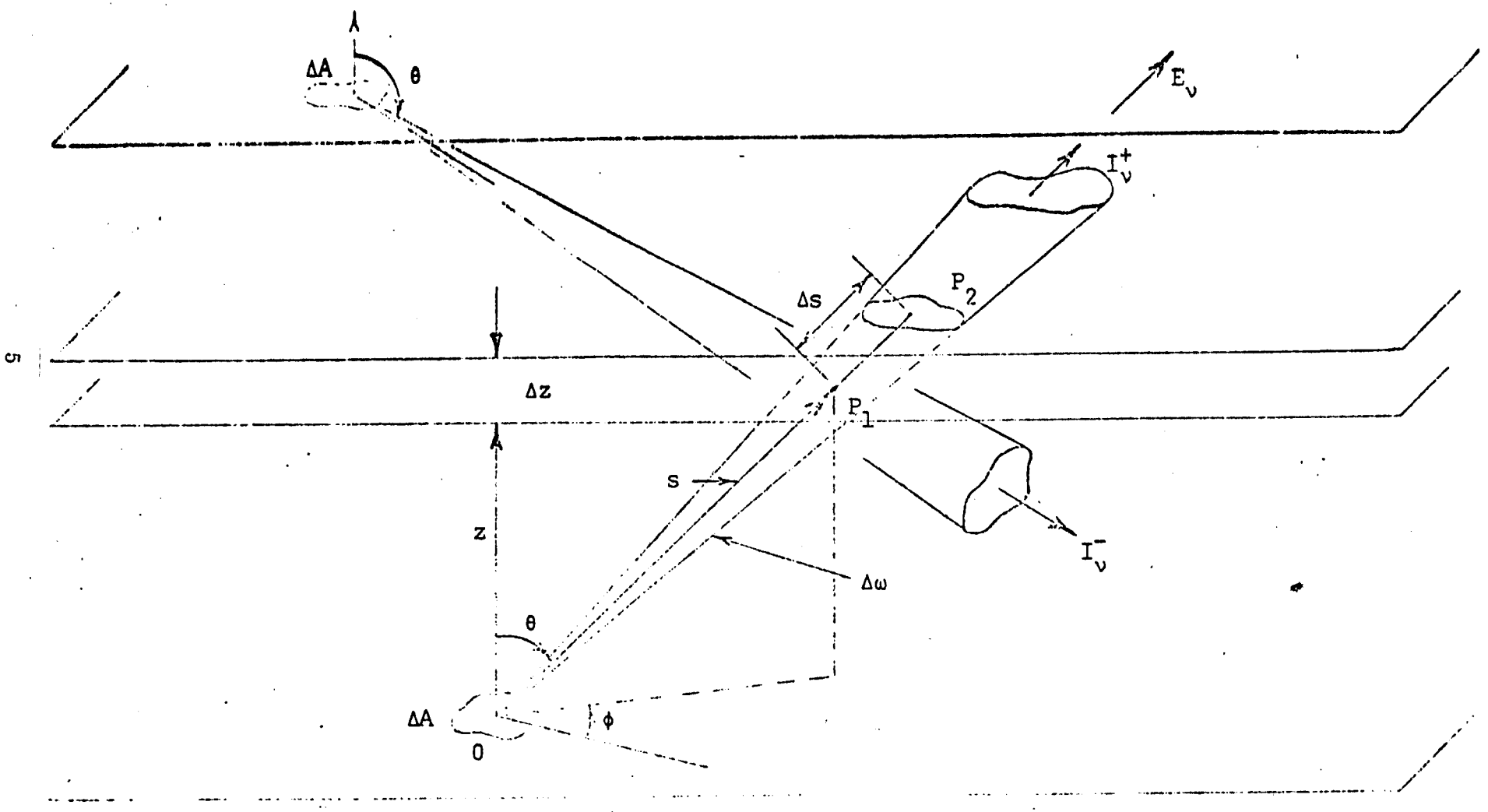

FIGURE 1: RADIATION TRANSFER FIELD GEOMETRY

length Δs and the incident intensity as follows:

$$\Delta I_\nu = -\kappa'_\nu \rho I_{\nu P_1} \Delta s,$$

where ΔI_ν is the change in intensity of the beam passing through Δm, the minus sign indicating a decrease in intensity. For thermodynamic equilibrium we have, by Kirchoff's law, $j_\nu = \kappa'_\nu \frac{e_{b\nu}}{\pi}$, where $e_{b\nu}$ represents the Planck function $e_{b\nu} \equiv \frac{2\bar{h}\nu^3}{c^2} \frac{\pi}{e^{\bar{h}\nu/kT} - 1}$ [2]. In addition, a scattering coefficient γ'_ν is defined such that the rate of energy in a frequency range $\Delta\nu$, which is scattered by Δm from an incident beam of intensity $I_{\nu P_1}$ is $\gamma'_\nu I_{\nu P_1} \Delta m \Delta\omega \Delta\nu$, where $\Delta\omega$ is the solid angle associated with $I_{\nu P_1}$. By applying the definitions of emission, absorption and scattering coefficients, the change in intensity as a beam crosses the atmospheric slab between points P_1 and P_2 may be shown to have the following form [3,4].

$$\Delta I_\nu = \rho j_\nu \Delta s - \rho \kappa'_\nu I_\nu(\theta,\phi,s)\Delta s + \frac{\rho\gamma'_\nu}{4\pi} \Delta s \int_{4\pi} p(\theta,\phi;\theta',\phi') I_\nu(\theta',\phi',s) d\omega'$$

$$-\gamma'_\nu I_\nu (\theta,\phi,s)\rho\Delta s, \qquad (1)$$

where $\Delta I_\nu \equiv I_\nu(\theta,\phi,s+\Delta s) - I_\nu(\theta,\phi,s)$.

In this equation $I_\nu(\theta',\phi',s)$ and $d\omega'$ denote intensity and solid angle, respectively, of a "secondary" beam, incident upon Δm, and which undergoes some scattering from the (θ',ϕ') direction into the direction (θ,ϕ) of the

"primary" beam associated with $d\omega$. Limits on the integral indicate that the integration takes into account scattering from all directions. The symbol $P(\theta,\phi;\theta',\phi')$ denotes the scattering function, which measures the probability that radiation from a beam $d\omega'$ will be scattered into the direction of $d\omega$. In general, therefore, P is a function of $\theta,\phi,\theta',\phi'$. The simplest and most extensively studied type of scattering assumes that scattering is uniform in all directions, i.e. that P=1. This assumption of isotropic scattering will be made here, although other scattering models could be employed without difficulty in the subsequent calculations. For a further discussion of isotropic and non-isotropic scattering, References 3 and 5 may be consulted.

Division of Eq. (1) by Δs, introduction of Kirchoff's law, and passage to the limit as $\Delta s \to 0$ produces the following differential equation for $I_\nu = I_\nu(\theta,\phi,s)$:

$$\frac{dI_\nu}{ds} + \beta'_\nu \rho I_\nu = \kappa'_\nu \rho \frac{e_{b\nu}}{\pi} + \frac{\gamma'_\nu \rho}{4\pi} \int_{4\pi} I_\nu(\theta',\phi',s)d\omega', \qquad (2)$$

in which P has been set to unity, and the definition of the extinction coefficient $\beta'_\nu \equiv \kappa'_\nu + \gamma'_\nu$ has been introduced. The definition of the optical thickness $\tau_\nu \equiv \int_0^z \beta'_\nu \rho dz'$ is now introduced. The notation $\mu \equiv \cos\theta$ is also introduced at this point. From these definitions it follows that, along the sensor line-of-sight,

$$\frac{dI_\nu}{ds} = \mu \frac{dI_\nu}{dz} = \rho \beta'_\nu \mu \frac{dI_\nu}{d\tau_\nu} \quad , \text{ where}$$

it is further assumed that the extinction coefficient is constant over the range of z under consideration. The derivative is replaced in Eq. (2) as indicated above, and the resulting equation is then divided by $\rho\beta'_\nu$. It is also convenient to replace the quantities $\kappa'_\nu\rho$, $\gamma'_\nu\rho$, and $\beta'_\nu\rho$ by the symbols κ_ν, γ_ν and β_ν, respectively. When these steps are taken, Eq. (2) becomes

$$\mu \frac{dI_\nu}{d\tau_\nu} + I_\nu = \frac{1}{\pi\beta_\nu}\left[\kappa_\nu e_{b\nu} + \frac{\gamma_\nu}{4}\int_{4\pi} I_\nu(\theta',\phi',\tau_\nu)d\omega'\right] . \qquad (3)$$

Equation (3) may be regarded as actually two equations, having exactly the same form, except that one equation is in terms of I_ν^+ and the other equation is in terms of I_ν^-. Boundary conditions for a beam whose intensity is described by Eq. (3) are taken to be

$$I_\nu^+\Big|_{\tau_\nu=0} = I_\nu^+(\theta,\phi); \qquad I_\nu^-\Big|_{\tau_\nu=\tau_{0\nu}} = 0 \quad ,$$

where $\tau_{0\nu}$ represents the uppermost value of τ_ν. This assumes that surface intensity is known and that there is no downward intensity at the uppermost elevation of the region under study. With these boundary conditions, formal "solutions" to the Eqs. (3) may be written as follows:

$$I_\nu^+(\theta,\phi,\tau_\nu) = I_{0\nu}^+(\theta,\phi)e^{-\tau\nu/\mu} + \frac{1}{\pi}\int_0^{\tau_\nu}\left[\frac{\kappa_\nu}{\beta_\nu}e_{b\nu} + \frac{\gamma_\nu}{\beta_\nu}\frac{G_\nu(\mu,\phi,t)}{4}\right]\frac{e^{-(\tau_\nu-t)/\mu}}{\mu}dt, \quad 0<\mu\leq 1$$

$$I_\nu^-(\theta,\phi,\tau_\nu) = -\frac{1}{\pi}\int_{\tau_\nu}^{\tau_{0\nu}}\left[\frac{\kappa_\nu}{\beta_\nu}e_{b\nu} + \frac{\gamma_\nu}{\beta_\nu}\frac{G_\nu(\mu,\phi,t)}{4}\right]\frac{e^{-(\tau_\nu-t)/\mu}}{\mu}dt, \quad -1\leq\mu<0 . \qquad (4)$$

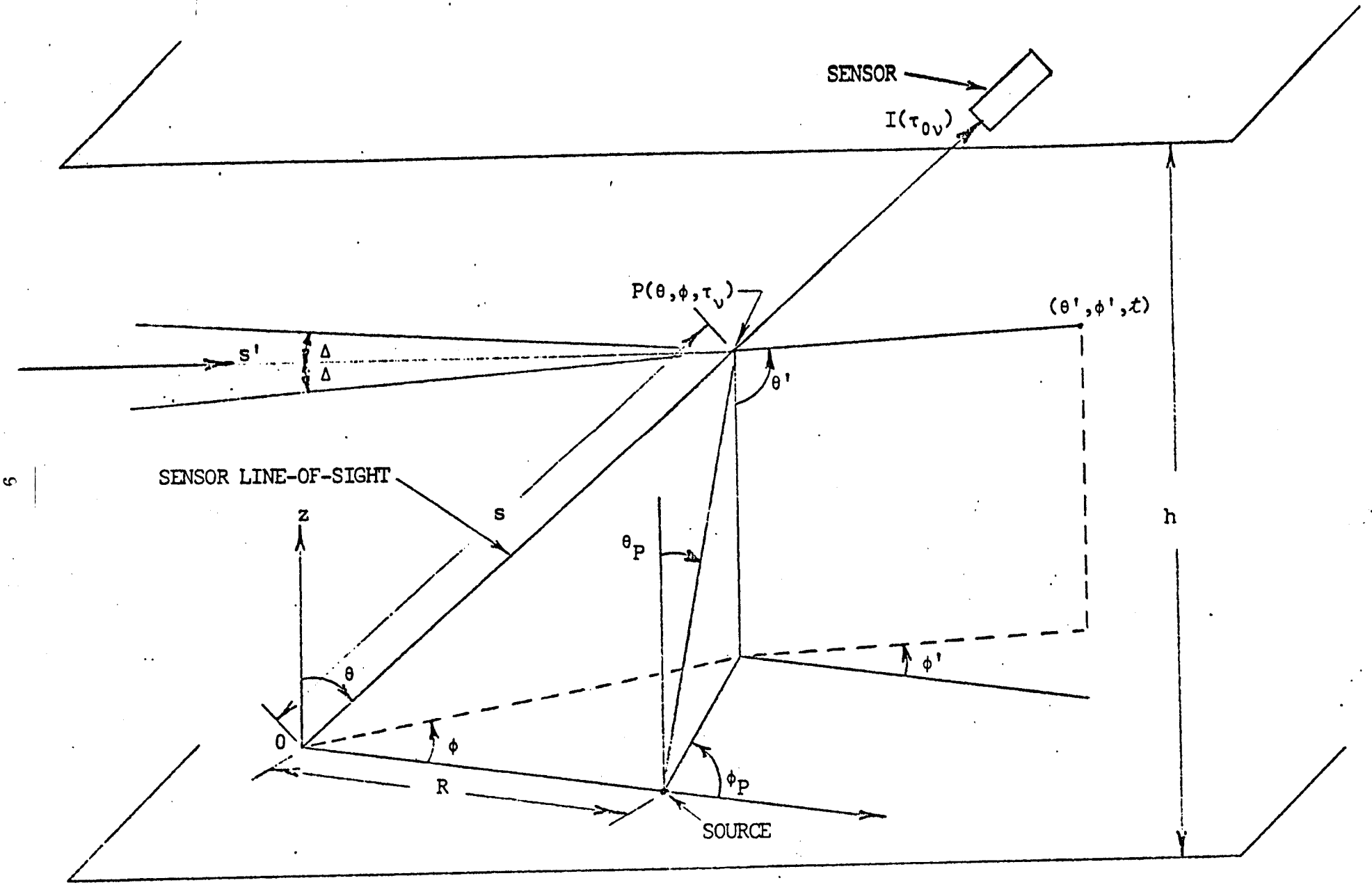

FIGURE 2: SENSOR/POINT SOURCE GEOMETRY

In Eqs. (4) t is a dummy variable of integration, and the notation

$$G_\nu(\mu,\phi,\tau_\nu) \equiv \int_{4\pi} I_\nu(\theta',\phi',\tau_\nu)d\omega'$$

is introduced. Equations (4) do not represent a true solution because of the presence of the G_ν term.

The relative contributions of κ_ν and γ_ν to the extinction coefficient are best described by the use of the scattering albedo $\bar{\omega}\equiv\frac{\gamma_\nu}{\beta_\nu}$. Thus $\kappa_\nu = 1-\bar{\omega}_\nu$.

Pure Scattering $(\bar{\omega}_\nu=1)$

In this case Eqs. (4) reduces to

$$I_\nu^+(\theta,\phi,\tau_\nu) = I_{0\nu}^+(\theta,\phi)e^{-\tau_\nu/\mu} + \frac{1}{4\pi}\int_0^{\tau_\nu} G_\nu(\theta,\phi,t)\,\frac{e^{-(\tau_\nu-t)/\mu}}{\mu}\,dt$$

$$I_\nu^-(\theta,\phi,\tau_\nu) = -\frac{1}{4\pi}\int_{\tau_\nu}^{\tau_{0\nu}} G_\nu(\theta,\phi,t)\,\frac{e^{-(\tau_\nu-t)/\mu}}{\mu}\,dt \quad . \qquad (5)$$

Equations (5) will now be employed to obtain a single integral equation in terms of G_ν. The expressions given by Eqs. (5) for I_ν^+ and I_ν^- are valid for $\mu\neq0$. Therefore for the numerical computation of G_ν at a point such as P (Fig. 2) the following approach is taken: The expressions given by Eqs. (5) for I_ν^+ and I_ν^- are employed in a region which excludes a small solid angle $\delta\omega$, within which $\frac{\pi}{2} - \xi \leq \theta \leq \frac{\pi}{2} + \xi$, $0 \leq \phi \leq 2\pi$, centered in a horizontal plane through the point. Contributions from within $\delta\omega$ are considered separately. The value of ξ is determined by numerical convergence requirements, to be considered in the following section.

To proceed with the development of the integral equation, G_ν is written in the following form:

$$G_\nu(\theta,\phi,\tau_\nu) = \int_{4\pi} I_\nu(\theta',\phi',\tau_\nu)d\omega' = \int_0^{2\pi}\int_0^{\pi} I_\nu(\theta',\phi',\tau_\nu)\sin\theta'd\theta'd\phi' \tag{6}$$

$$= \int_0^{2\pi}\int_0^{\pi/2-\xi} I_\nu^+(\theta',\phi',\tau_\nu)\sin\theta'd\theta'd\phi' + \int_0^{2\pi}\int_{\pi/2+\xi}^{\pi} I_\nu^-(\theta',\phi',\tau_\nu)\sin\theta'd\theta'd\phi' + \int_{\delta\omega} I_\nu^H d\omega \ .$$

The solid angle $\delta\omega$ is taken to be small enough so that the intensity I_ν^+ appearing in the right-hand integral lies, to a close approximation, in a horizontal plane. Letting s denote distance measured in the horizontal plane, a development completely analogous to that leading to Eq. (2) produces the following equation:

$$\frac{dI_\nu^H(s)}{ds} + \beta_\nu I_\nu^H(s) = \frac{\beta_\nu}{4\pi} G_\nu(s) \ , \tag{7}$$

$$\text{from which} \quad I_\nu^H(s) = \frac{1}{4\pi}\int_{-\infty}^{s} G_\nu(s')e^{-\beta_\nu(s-s')}\,\beta_\nu ds' \ . \tag{8}$$

Equation (7) and (8) are now introduced into Eq. (6), giving

$$G_\nu(\theta,\phi,\tau_\nu) = \int_0^{2\pi}\int_0^{\pi/2-\xi} I_{0\nu}^+(\theta',\phi')e^{-\tau_\nu/\mu'}\sin\theta'd\theta'd\phi'$$

$$+ \frac{1}{4\pi}\int_0^{2\pi}\int_0^{\pi/2-\xi}\int_0^{\tau_\nu} G_\nu(\theta',\phi',t)\frac{e^{-(\tau_\nu-t)/\mu'}}{\mu'}\sin\theta'dtd\theta'd\phi' \tag{9}$$

$$-\frac{1}{4\pi}\int_0^{2\pi}\int_{\pi/2+\xi}^{\pi}\int_{\tau_\nu}^{\tau_{0\nu}} G_\nu(\theta',\phi',t)\frac{e^{-(\tau_\nu-t)/\mu'}}{\mu'}\sin\theta'dtd\theta'd\phi' + \int_{\delta\omega}\int_{-\infty}^{s}\frac{1}{4\pi} G_\nu(s')e^{-\beta_\nu(s-s')}\beta_\nu ds'd\omega \ .$$

This equation may be written in the following form:

$$G_\nu(\mu,\phi,\tau_\nu) = \int_0^{2\pi}\int_\Delta^1 I_{0\nu}^+(\mu',\phi')e^{-\tau_\nu/\mu'}\,d\mu'd\phi' + \frac{1}{4\pi}\int_0^{2\pi}\int_\Delta^1\int_0^{\tau_\nu} G_\nu(\mu',\phi',t)\frac{e}{\mu'}^{-(\tau_\nu-t)/\mu'}\,dtd\mu'd\phi'$$

$$+ \frac{1}{4\pi}\int_0^{2\pi}\int_{-\Delta}^{-1}\int_{\tau_\nu}^{\tau_{0\nu}} G_\nu(\mu',\phi',t)\frac{e}{\mu'}^{-(\tau_\nu-t)/\mu'}\,dtd\mu'd\phi' + \int_{\delta\omega}\int_{-\infty}^{s}\frac{1}{4\pi}G_\nu(s')e^{-\beta_\nu(s-s')}\,\beta_\nu ds'd\omega\ , \tag{10}$$

where $\Delta(>0)$ represents the minimum value of μ'. The first integral on the right side of Eq. (10) may be evaluated in view of the assumption that emission from the surface proceeds from a single point source, with the remainder of the surface assumed black and nonemitting. Let $I_{0\nu}$ denote the intensity at the surface point source, and let $\tau_{\nu P}$, ϕ_P and μ_P denote optical thickness, direction cosine and polar angle, respectively, of a beam directed from the point source to a point P, on the sensor line-of-sight, at which the evaluation of the integral is to be made. The integral is evaluated as follows:

$$\int_0^{2\pi}\int_\Delta^1 I_{0\nu}^+(\theta',\phi')e^{-\tau_\nu/\mu'}\,d\mu'd\phi' = \lim_{\varepsilon\to 0^+}\int_{\phi_P-\frac{\varepsilon}{2}}^{\phi_P+\frac{\varepsilon}{2}}\int_{\mu_P-\frac{\varepsilon}{2}}^{\mu_P+\frac{\varepsilon}{2}} I_{0\nu}\frac{e}{\varepsilon^2}^{-\tau_{\nu P}/\mu_P}\,d\mu'd\phi' \tag{11}$$

$$= I_{0\nu}e^{-\tau_{\nu P}/\mu_P} \equiv G_\nu^*(\mu,\phi,\tau_\nu)\ .$$

The method of successive substitutions [6] is used to obtain approximate solutions to Eq. (10). In this method it is first observed that an expression for $G_\nu(\mu',\phi',t)$ may be written in a manner completely analogous to Eq. (10).

This expression is substituted into the right side of Eq. (10), and it is observed that the substitution process may again be performed. Repeated substitutions are carried out in this manner, with the higher order terms representing the contribution from higher degrees of multiple scattering. To proceed, the expression for $G_\nu(\mu',\phi',t)$ is written, using Eqs. (10) and (11) as follows:

$$G_\nu(\mu',\phi',t) = G^*_\nu(\mu',\phi',t) + \frac{1}{4\pi}\int_0^{2\pi}\int_\Delta^1\int_0^t G_\nu(\bar{\mu},\bar{\phi},\bar{t})\frac{e^{-(t-\bar{t})/\bar{\mu}}}{\bar{\mu}}\, d\bar{t}d\bar{\mu}d\bar{\phi}$$

$$+\int_0^{2\pi}\int_{-\Delta}^{-1}\int_t^{\tau_{0\nu}} G_\nu(\bar{\mu},\bar{\phi},\bar{t})\frac{e^{-(t-\bar{t})/\bar{\mu}}}{\bar{\mu}}\, d\bar{t}d\bar{\mu}d\bar{\phi} + \int_{0\omega}\int_{-\infty}^{\bar{s}} \frac{1}{4\pi} G_\nu(\bar{s}')e^{-\beta_\nu(\bar{s}-\bar{s}')}\, \beta_\nu d\bar{s}'d\omega \quad . \tag{12}$$

This successive substitution produces the following series:

$$G_\nu(\mu,\phi,\tau_\nu) = G^*_\nu(\mu,\phi,\tau_\nu) + \frac{1}{4\pi}\left[\int_0^{2\pi}\int_\Delta^1\int_0^{\tau_\nu} G^*_\nu(\mu',\phi',t)\frac{e^{-(\tau_\nu-t)/\mu'}}{\mu'}\, dtd\mu'd\phi'\right.$$

$$\left. +\int_0^{2\pi}\int_{-\Delta}^{-1}\int_{\tau_\nu}^{\tau_{0\nu}} G^*_\nu(\mu',\phi',t)\frac{e^{-(\tau_\nu-t)/\mu'}}{\mu'}\, dtd\mu'd\phi'\right] \tag{13}$$

$$+\int_{0\omega}\int_{-\infty}^{s} \frac{1}{4\pi} G^*_\nu(s')e^{-\beta_\nu(s-s')}\, \beta_\nu ds'd\omega + \frac{1}{(4\pi)^2}\ (\quad) + \cdots \quad .$$

Each term of the series of triple integrals in Eq. (13) will be less than the corresponding term in the series

$$S \equiv \sum_{N=0}^{\infty} I_{0\nu}\left[\tau_{0\nu}\frac{(1-\Delta)}{2\Delta}\right]^N ,$$

which is convergent when $\frac{\tau_{0\nu}(1-\Delta)}{2\Delta} < 1$, i.e., when

$$\Delta > \frac{1}{1 + \frac{2}{\tau_{0\nu}}} \tag{14}$$

Also, the integral in Eq. (13) over $\delta\omega$ may be shown to be less than $\frac{I_{0\nu}\Delta}{2}$.

Numerical Results

Convergence, in the sense of numerical accuracy to a desired number of significant figures, was found to exist for values of Δ considerably smaller than those predicted by Eq. (14), however. For the computational phase of the investigation a value of Δ=0.01 was found to provide the most efficient means of obtaining numerical results, in that the rate of convergence of the series of triple integrals in Eq. (13) was acceptable, while the contribution due to the integral over $\delta\omega$ was small enough to be neglected. Moreover, for the range of optical thicknesses studied, the multiple-scattering terms proportional to $\frac{1}{(4\pi)^2}$ or higher-order terms provided negligible contributions to the value of G_ν.

For computational purposes a truncation of Eq. (13) after the terms proportional to $\frac{1}{4\pi}$ was used to compute values of G_ν, which were then inserted into Eq. (5), in order to find values of I_ν^+ at $\tau_\nu=\tau_{0\nu}$. To proceed with the numerical integration of Eq. (13) it is necessary to determine the expression for $G_\nu^*(\mu',\phi',t)$ as a function of the μ', ϕ' and t coordinates and the location of the point such as P in Fig. 2, at which the value of G_ν is to be computed. From the geometry of Fig. 2 the following expression is obtained:

$$G_\nu^*(\mu',\phi',t) = I_{0\nu} \times \exp\left[\left(\beta_\nu s\sqrt{1-\mu^2}\cos\phi + \frac{\beta_\nu s\mu - t}{\mu'}\sqrt{1-\mu'^2}\cos\phi' - \beta_\nu R\right)^2 + \left(\beta_\nu s\sqrt{1-\mu^2}\sin\phi + \frac{\beta_\nu s\mu - t}{\mu'}\sqrt{1-\mu'^2}\sin\phi'\right)^2 + t^2\right]^{-0.5} \tag{15}$$

The reference direction for the angle ϕ' is taken to be the same as that for ϕ, namely, parallel to the line from the sensor line-of-sight ground intercept to the point source.

The elementary trapezoidal rule of integration was determined to be the most efficient method for treating the multiple integrals, with a Simpson's rule technique used for integration along the sensor line-of-sight. Figures 3 through 6 display the results of the numerical computations. The symbols $\mu(=\cos\theta)$, R and ϕ refer to the orientation of the sensor line-of-sight with respect to the point source (Fig. 2). In these figures it is assumed that the sensor line-of-sight does not intercept the ground at the point source itself. Thus the first term on the right side of Eq. (5) is taken to be zero in the computations leading to Figs. 3 through 6. For the special case in which the sensor line-of-sight does pass through the point source, the dimensionless intensity $\frac{I(\tau_{0\nu})}{I_{0\nu}}$ may be obtained by adding the quantity $e^{-\tau_{0\nu}/\mu}$ to values obtained from Figs. 3 through 6, evaluated at $\frac{R}{h} = 0$.

Conclusions

The numerical results displayed in Figs. 3 through 6 indicate that, as expected, the effect of the point source upon the intensity decreases with decreasing optical thickness. For a constant optical depth, however, the effect of atmospheric participation increases with decreasing values of μ, with the rate of increase greater for greater optical depths.

The effect of the variable $\frac{R}{h}$ is relatively slight, especially when $\tau_{0\nu}$ is small or the sensor line-of-sight is nearly vertical. For

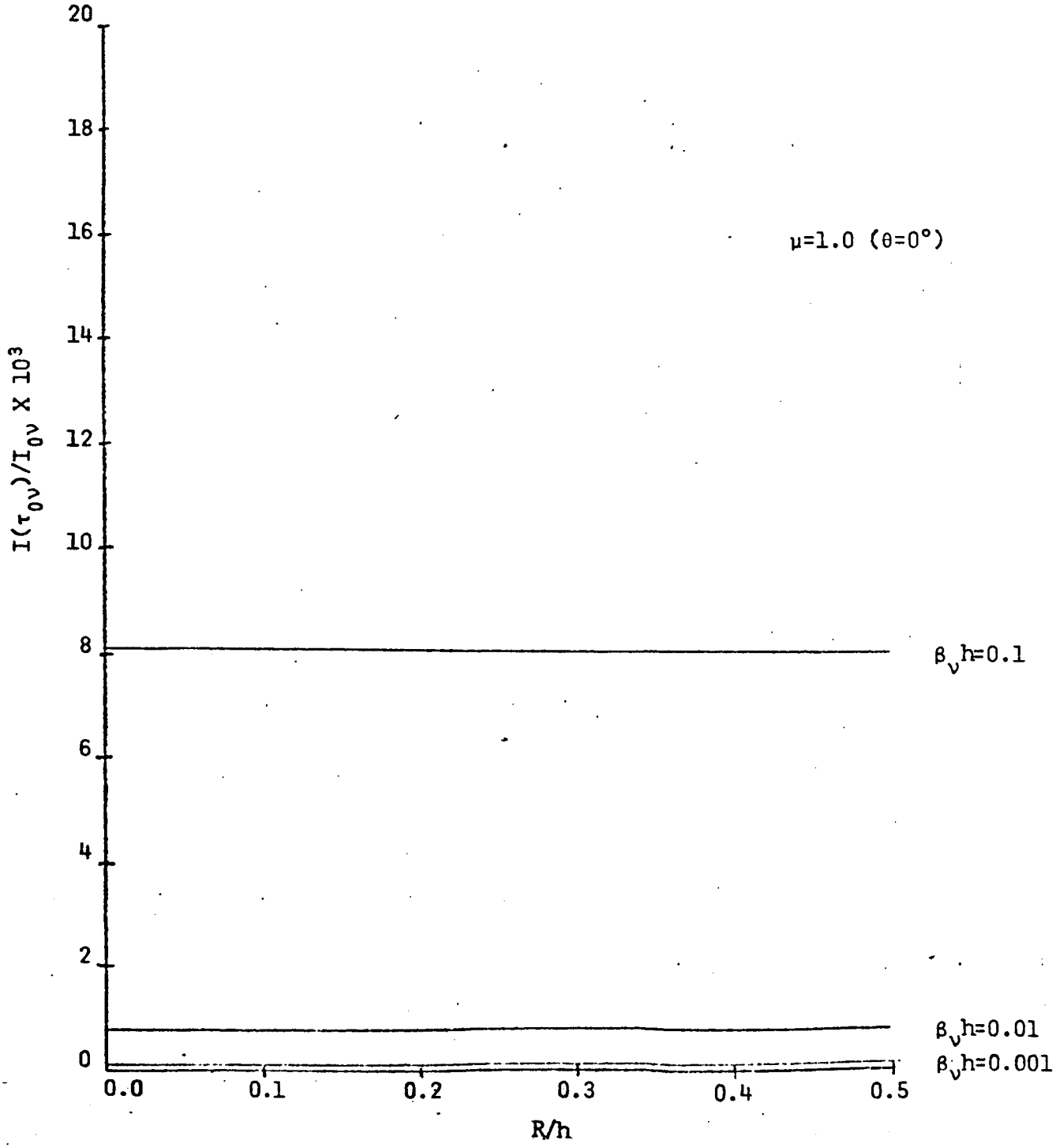

FIGURE 3: DIMENSIONLESS INTENSITY VS. R/h AS FUNCTION OF OPTICAL DEPTH, θ=0°

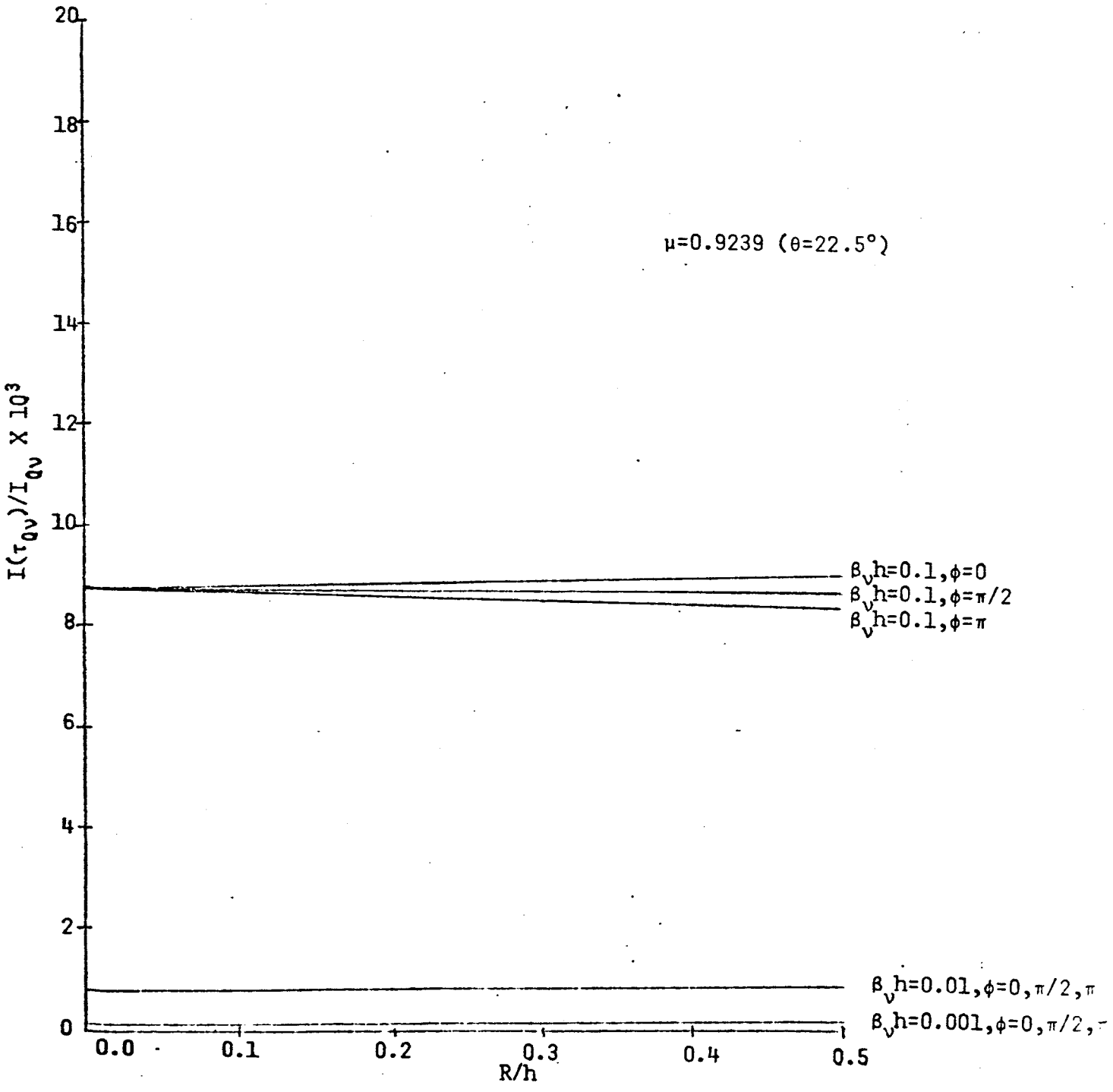

FIGURE 4: DIMENSIONLESS INTENSITY VS. R/h AS FUNCTION OF OPTICAL DEPTH & φ, θ=22.5°

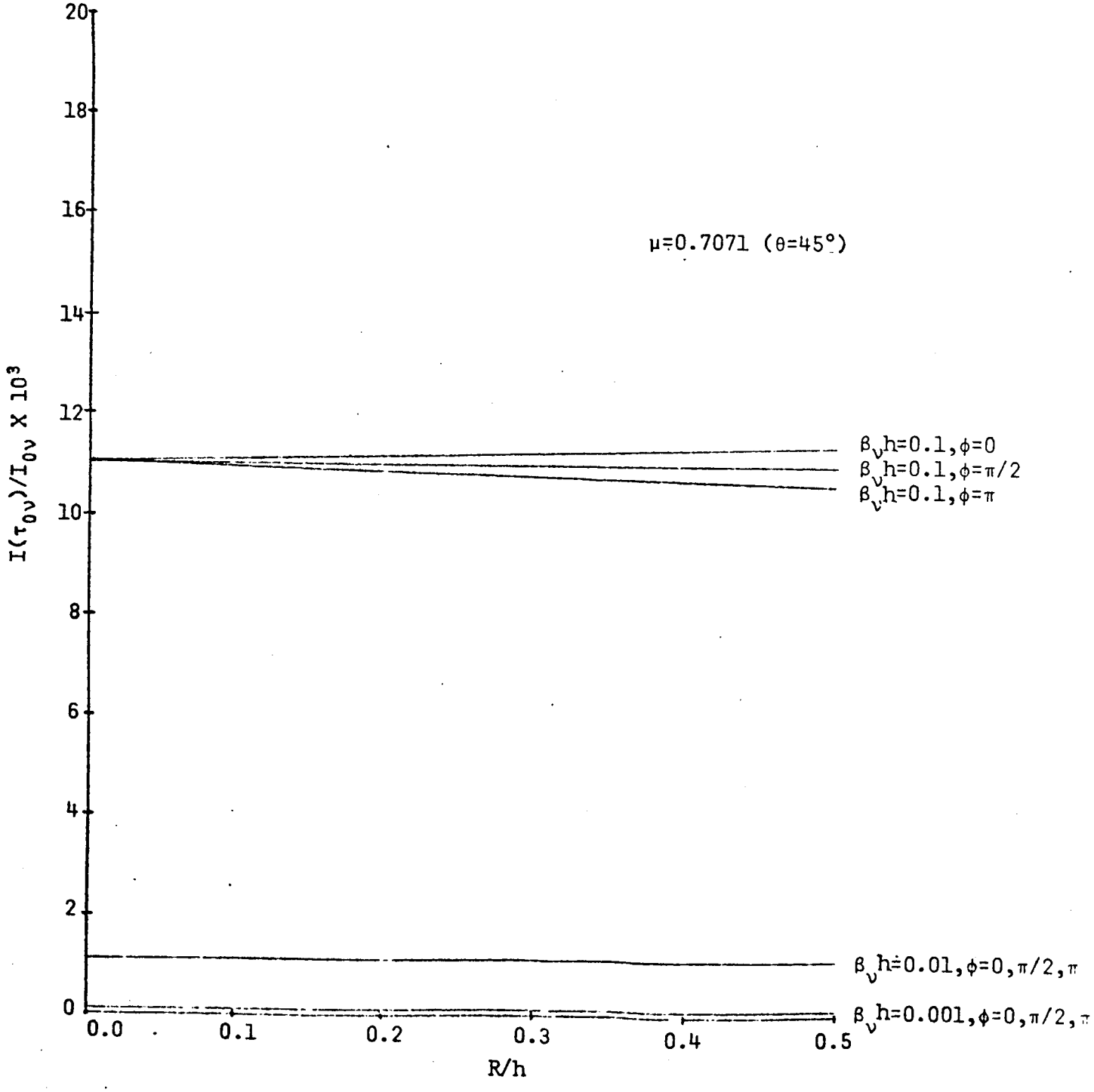

FIGURE 5: DIMENSIONLESS INTENSITY VS. R/h AS FUNCTION OF OPTICAL DEPTH & ϕ, θ=45°

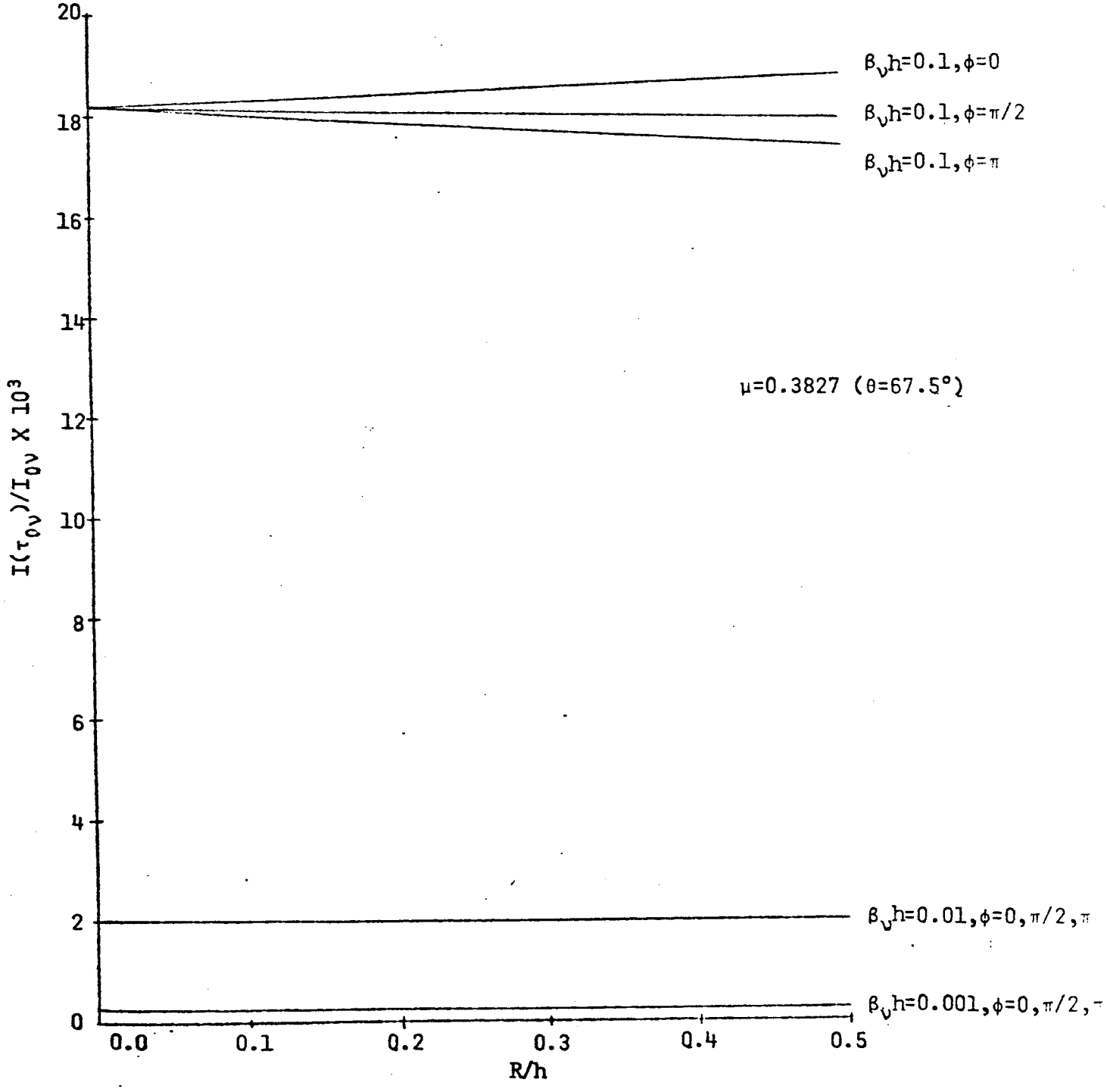

FIGURE 6: DIMENSIONLESS INTENSITY VS. R/h AS FUNCTION OF OPTICAL DEPTH & ϕ, θ=67.5°

larger values of $\tau_{0\nu}$ and smaller values of μ, however the dimensionless intensity shows some variation with $\frac{R}{h}$.

III. DISCUSSION OF RESULTS

The data presented in Figs. 3 through 6 are the results obtained by solving the equations of transfer for a plane-parallel, scattering atmosphere (no absorption or emission). In addition, it was assumed that the only energy source on the earth surface is a single point source (Fig. 2), and so the energy incident on the sensor is that which was scattered into the line-of-sight (except in the special case when the sensor line-of-sight passes through the source).

$I(\tau_{0\nu})$ is a measure of the energy incident on the sensor while $I_{0\nu}$ is a measure of the energy emitted by the point-source, the latter being a function of the point-source temperature. The ratio $I(\tau_{0\nu})/I_{0\nu}$ is plotted vs. $\frac{R}{h}$ which, for a given h (altitude), represents the distance from the source to the sensor line-of-sight ground intercept. On each plot are results for various values of the optical thickness $\beta_\nu h$, which for a fixed altitude increases as the scattering coefficient increases. The results thus show that as the scattering coefficient increases, more scattered energy is received by the sensor. Also, when $\theta \neq 0°$, the data are plotted for various values of ϕ, which specifies the orientation of the horizontal projection of the sensor line-of-sight with respect to a line from the point source to the sensor line-of-sight ground intercept (Fig. 2). Finally, each figure represents a different value of θ, which is the displacement angle of the sensor line-of-sight from the vertical.

The results, then, clearly indicate, as expected, that as the scattering tendency of the atmosphere increases, so does the energy level, $I(\tau_{0\nu})$, received by the sensor. Also, this effect is almost constant, for a given $\beta_\nu h$ with respect to $\frac{R}{h}$. Figures 5 and 6 do indicate that $I(\tau_{0\nu})/I_{0\nu}$ varies somewhat with $\frac{R}{h}$ and ϕ for the higher scattering conditions.

As an example of how these results might be applied, assume that the sensor at an altitude of 100 km is viewing the surface of the earth at an angle of 67.5° from the vertical (θ=67.5°) and that the earth surface is zero degrees absolute (i.e. emits no radiant energy) except for one point which is 20 km from the sensor line-of-sight ground intercept ($\frac{R}{h}$=0.2) and lies directly under the sensor line-of-sight (ϕ=0°). This example is pictured in Fig. 7. In the absence of scattering, the sensor would receive no energy since it looks at a zero degree absolute surface, i.e. $I(\tau_{0\nu})$ would be zero. However, examination of Fig. 6 indicates that if $\beta_\nu h$=0.1, then $I(\tau_{0\nu})/I_{0\nu}=18.5 \times 10^{-3}$. Since $I_{0\nu}$ is not zero, it is clear that $I(\tau_{0\nu})$ is not zero and so the sensor would "predict" a false temperature. Moreover, a false reading would also be indicated by a sensor attempting to remotely measure the temperature of an emitting source located at the sensor line-of-sight ground intercept due to the presence of the aforementioned "disturbing" source.

The present analysis has included several simplifying assumptions, and continued analysis is required to include additional considerations. However, it is clear that a non-uniform (non-isothermal) earth surface will affect the sensing of the earth surface, the magnitude of the effect depending on the atmospheric conditions and the sensor/point-source orientation.

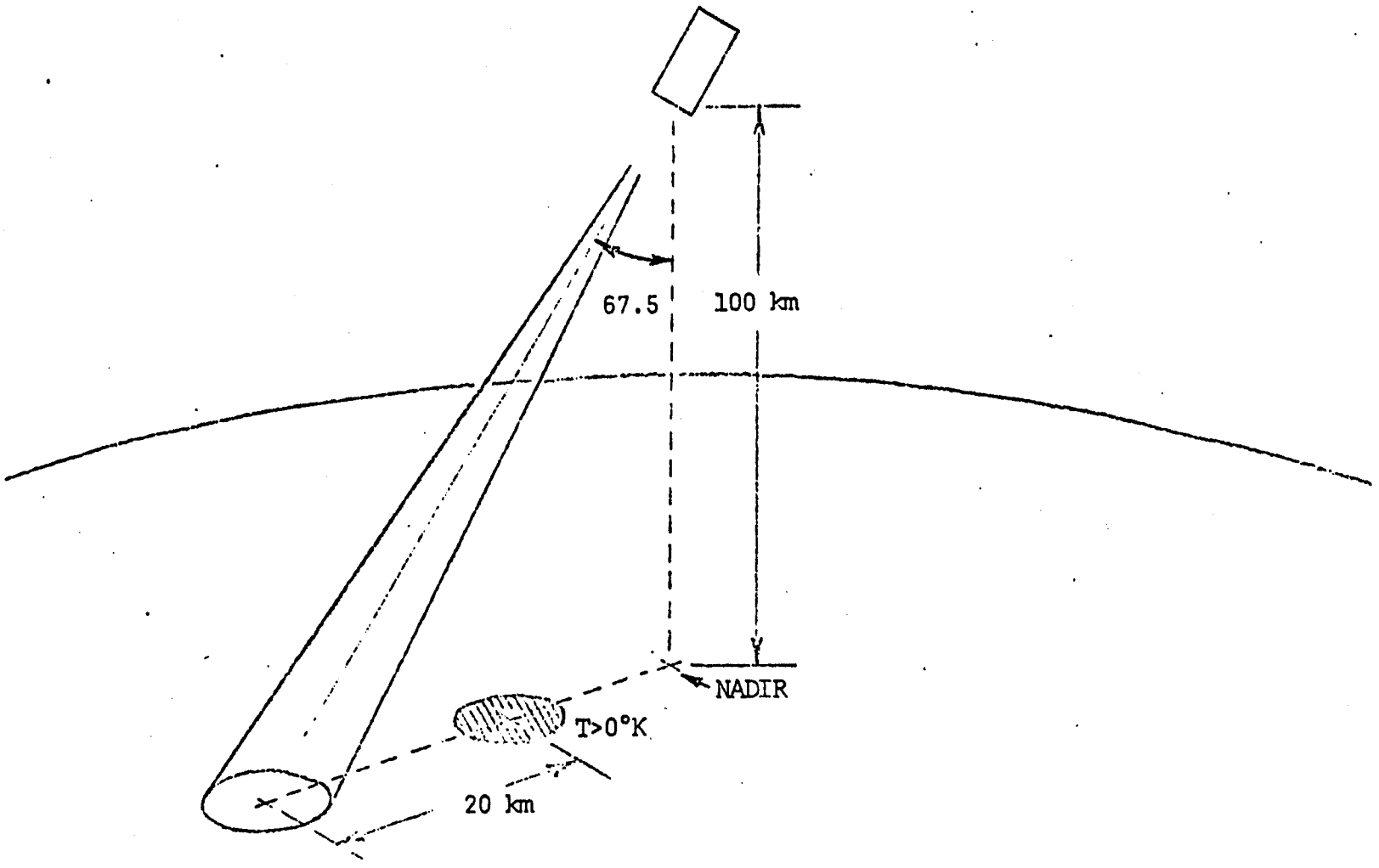

FIGURE 7: EXAMPLE APPLICATION

IV. ATMOSPHERIC AND RADIATION TRANSFER PROPERTIES

As indicated in Section II, the results obtained thus far are in the form of dimensionless groups. However, for ultimate interpretation of results for operational situations, the radiation transfer properties of the atmosphere must eventually be known. These properties include the molecular absorption coefficients and the absorption and scattering coefficients due to haze, dust, clouds, etc. The molecular constituents important in the infrared region are H_2O, CO_2, O_3, CH_4, CO and N_2O. In addition to the molecular absorption, scattering and absorption due to dust, haze, and clouds are significant in the infrared region [7] although computation of scattering coefficients, especially for dust and clouds, is quite complex.

Another factor in the process of obtaining radiation transfer properties is that they are functions of such variables as the local pressure, temperature, density, and molecular concentrations, so that profiles of these atmospheric properties must be known before the appropriate scattering and absorption coefficients can be determined. The four-dimensional atmospheric models [1] which predict moisture, temperature, density, and pressure profiles as functions of latitude, longitude, altitude, and time, will be used as input to existing radiation transfer property models. These existing radiation transfer property models will then generate scattering and absorption coefficients required for the transfer analysis presented

in Section II. Since the 4-D models predict atmospheric conditions up to 25 km on a world-wide basis, they should be most useful in analysis of ERTS-B and SKYLAB sensor performance over various locations.

Anding, et al. [8] has developed the capability to compute molecular absorption coeffients and haze absorption and scattering coefficients and cloud extinction coefficients in the course of an investigation of atmospheric effects on determination of sea-surface temperatures. It is anticipated that this work will be used extensively in future phases of the present study.

V. SKYLAB EARTH SENSING EXPERIMENTS

SKYLAB will carry the Earth Resources Experiment Package (ERFP) during its 1973 mission and the two sensors which will be discussed relative to this study are 1) the infrared Spectrometer, designated S191, and 2) the Multispectral Scanner, designated S192 [9]. The Infrared Spectrometer (S191) will sense reflected energy as a function of wavelength in the .4 to 2.4 μm range and emitted energy as a function of wavelength in the 6.2 to 15.5 μm range with a nominal field of view of 1 milliradian (¼ N. mi diameter circle at nadir).

The Multispectral Scanner (S192) measures reflected energy in twelve separate channels (wavelength bands) and emitted energy in one channel (10.2 to 12.5 μm). The instantaneous field of view of S192 is 0.182 milliradians (an area 260 ft. across) and the thermal channel (10.2 to 12.5 μm) is designed to measure emitted energy with sufficient accuracy to be able to measure surface temperatures within approximately 0.5°K.

It is anticipated that results of either of these experiments can be used to verify the results of this analytical study. For example, consider Fig.8. This figure depicts a sensor aimed at the nadir with a field-of-view covering an area on the ground of A_s. This configuration would represent S191 when it is aimed at the nadir or S192 when its scan angle is 0° (and the scan line crosses the nadir). The analysis presented in Section II is valid for any orientation of the solid angle subtended by A_s, i.e. any scan angle of S192 or any angle off the nadir for S191.

Note in Fig. 8 the area A' which is located a distance R from A_s. Some of energy emanating from this area will be scattered into the solid angle subtended by A_s. Therefore, not only will the sensor, e.g. S191, detect an erroneous energy input from A_s due to absorption and scattering of energy but also, energy originating at A' (i.e. outside the sensor field-of-view) will be scattered into the field-of-view producing additional error. It is obvious that the effect of A' on the sensor performance as it views A_s will depend on (1) the temperature difference between A_s and A' (2) the distance between A_s and A', and (3) the state of the atmosphere between the ground and the sensor.

The analysis developed in Section II allows each of the above to be varied independently and Fig. 3 shows results of the initial analysis for the vertical or 0° scan angle. It appears that the results of S191 and S192 from planned experiments can be used to verify the analytical results presented in this report. Since the requirements for the analysis are quite flexible, it is anticipated that the comparison between SKYLAB data and the results from this analysis can be made. However, it will be necessary to have accurate atmospheric data and accurate radiation property data as input to the present transfer model. The 4-D atmospheric models and the Anding radiation property models will be used to generate the appropriate data.

With favorable evaluation of the present transfer model, it will be possible to use the 4-D models, Anding property evaluations, and the transfer model presented here to plan sensor operation for future NASA missions. In other words, when atmospheric conditions exist, which the analysis predicts would lead to unacceptable error in sensor output, the experiment could be rescheduled, saving critical power, film, crew time, etc.

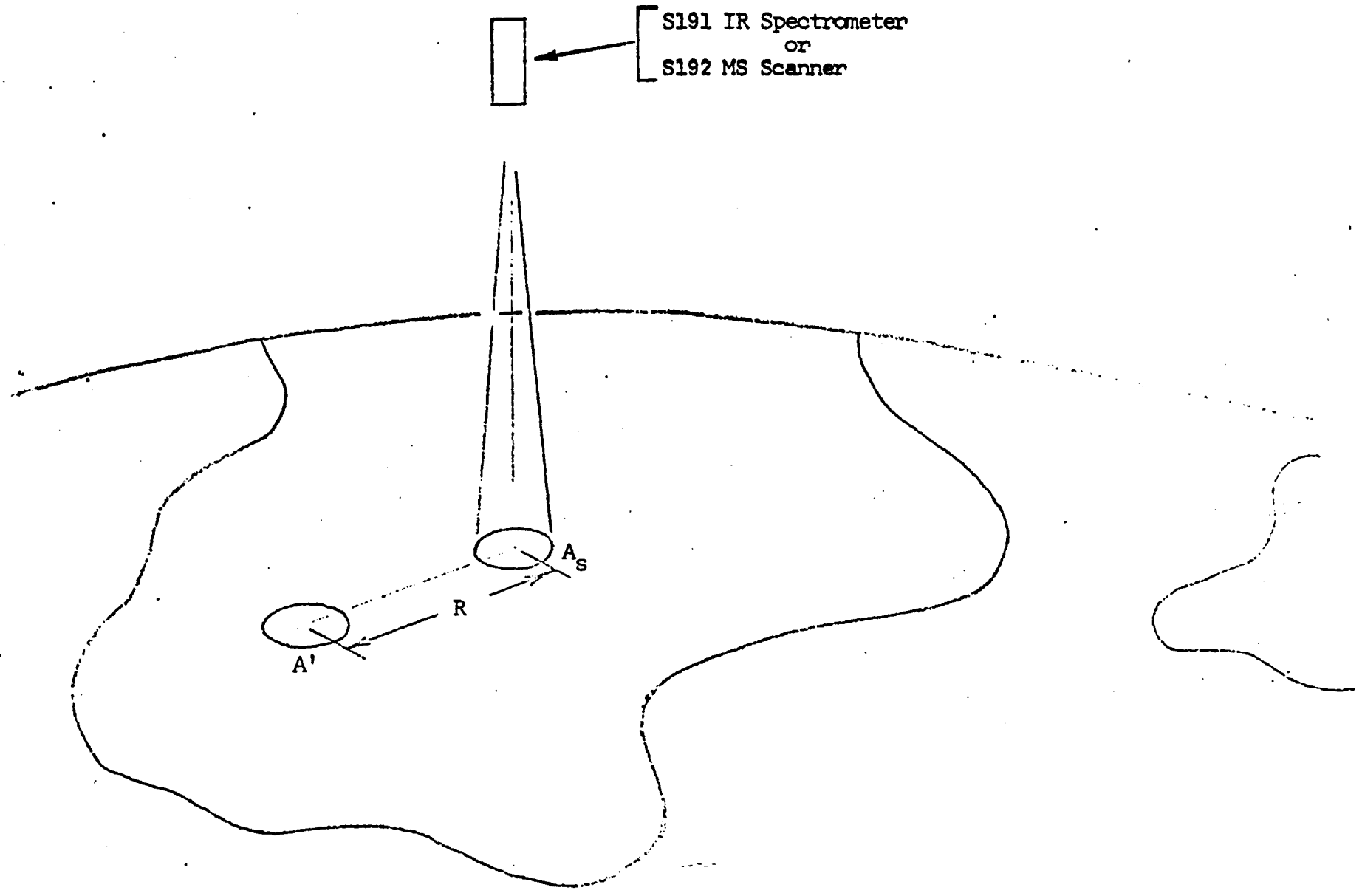

FIGURE 8: SKYLAB SENSOR ORIENTATION

VI. SUMMARY

Solutions of the plane-parallel, scattering atmosphere model, with a point-source of energy on the lower bounding surface, clearly indicate that a sensor operation in or above the earth's atmosphere will detect energy originating from a target on the ground even though the target is not in the sensor field-of-view. The amount of energy detected is a function of optical depth and sensor orientation with respect to the emitting point source.

The next phase of this investigation will be concerned with 1) including absorption and emission effects in the transfer model, and 2) including actual atmospheric parameters in the solutions. Successful completion of the next phase will allow investigation of SKYLAB and ERTS experiments.

REFERENCES

1. Spiegler, D. B. and Greaves, J. R., Development of Four-Dimensional Atmospheric Models (Worldwide), NASA CR-61352, Allied Research Associates, Inc., Concord, Mass., 1971.

2. Planck, M., The Theory of Heat Radiation, Dover Publications, New York, 1959.

3. Chandrasekhar, S., Radiative Transfer, Dover, 1960.

4. Sparrow, E. M. and Cess. R. D., Radiation Heat Transfer, Brooks/Cole Publishing Company, 1966.

5. Van De Hulst, Light Scattering by Small Particles, John Wiley & Sons, Inc., 1957.

6. Lovitt, V. M., Linear Integral Equations, Dover Publications, 1950.

7. Goody, R. M., Atmospheric Radiation, Oxford, 1964.

8. Anding, D., Kauth, R., and Turner, R., "Atmospheric Effects on Infrared Multispectral Sensing of Sea-Surface Temperature From Space," NASA CR-1858, July 1971.

9. SKYLAB-A/EREP Users Handbook, NASA-S-72-831-V, April 1972.